

People's Democratic Republic of Algeria
Ministry of Higher Education and Scientific Research
Mohamed El Bachir El Ibrahimi University of Borj Bou Arreridj
Faculty of Mathematics and Informatics
Informatics Department



DISSERTATION

Presented in fulfillment of the requirements of obtaining the degree
Master in Informatics
Specialty: Business Intelligence

THEME

Brain Tumor Detection Using U-Net and SVM

Presented by:

BENGUEZZOU Mohammed

BENYAHIAOUI Mohamed Assil

Publicly defended on: jj/mm/aaaa

In front of the jury composed of:

President:

Examiner:

Supervisor: Dr. ZOUAOUI Hakima

2024/2025

Dedication

To the architects of my dreams, my parents, whose unwavering love and guidance have been my compass; to my family, the sanctuary of my heart, and to my friends, the sparks of joy in my journey.

This thesis is a testament to your belief in me, a reflection of your sacrifices, and a celebration of the bond we share. Thank you for being my pillars of strength and my endless source of inspiration.

- Mohammed

Dedication

To my parents, whose unwavering love, support, and guidance have been instrumental in shaping my dreams; to my family, who have been my rock and my safe haven; and to my friends, who have been the source of joy and laughter in my life.

This thesis is a reflection of their sacrifices, a testament to their faith in me, and a celebration of the bond we share. Thank you for being my pillars of strength and my endless source of inspiration.

- Assil

Acknowledgments

Above all, we would like to thank GOD for granting health, the possibility and the will to start and continue our studies.

We would first like to thank to our supervisor, **Dr. Hakima Zouaoui**, forgiving us the chance to do our research and for providing invaluable guidance throughout this research. Also, we would acknowledge her for her generosity, her kindness, her knowledge, the time she gave us and her great availability which she showed us; made our task a lot easier.

We would also like to express our thanks to the members of the jury who honored us by participating in the examination of this work and enriching it with their proposals **Dr. !!!!!!!** and **Dr. !!!!!!!**.

In addition, we would like to acknowledge our parents for their love, care, prayers, sacrifices and for being always there for us

Abstract

Brain tumors, particularly gliomas, pose a significant clinical challenge, requiring both precise localization and accurate grading to guide treatment. Accurate segmentation of tumor regions is a critical first step, enabling meaningful analysis and interpretation of the affected areas. In this project, we present a hybrid framework that first segments tumor regions in brain Magnetic Resonance Imaging (MRI) scans using a U-Net model trained on the Brain Tumor Segmentation dataset, and then classifies these regions as Low-Grade or High-Grade Gliomas with a Support Vector Machine (SVM) model based on features extracted from the segmented masks. On the held-out test set, our U-Net achieved an accuracy of 99.3%, while the SVM classifier delivered an overall accuracy of 93%.

Keywords: Brain Tumor, U-Net, SVM, MRI, BraTS, Segmentation.

Résumé

Les tumeurs cérébrales, en particulier les gliomes, posent un défi clinique important, nécessitant à la fois une localisation précise et un classement précis pour guider le traitement. La segmentation précise des régions tumorales est une première étape essentielle, permettant une analyse et une interprétation significatives des zones touchées. Dans ce projet, nous présentons un cadre hybride qui segmente d'abord les régions tumorales dans l'imagerie par résonance magnétique (IRM) du cerveau en utilisant un modèle U-Net formé sur le jeu de données de segmentation des tumeurs cérébrales, puis classe ces régions comme faibleGliomes de grade ou de haut grade avec un modèle SVM (Support Vector Machine) basé sur les caractéristiques extraites des masques segmentés. Sur l'ensemble de test non exécuté, notre U-Net a atteint une précision de 99,3

Mots-clés: Tumeur cérébrale, U-Net, SVM, IRM, BraTS, Segmentation.

ملخص

تُشكل أورام الدماغ، وخاصة الأورام الدبقية، تحدياً طبياً كبيراً، وتتطلب إلى التحديد والتصنيف بشكل دقيق من أجل توجيه العلاج. إن التقسيم الدقيق لمناطق الورم يعد خطوة أولى بالغة الأهمية، حيث يتيح إجراء تحليل وتفسير مفيد للمناطق المصابة. في هذا المشروع، نقدم إطاراً هجيناً يقوم أولاً بتقسيم مناطق الورم في عمليات مسح (MRI) للدماغ باستخدام نموذج (U-Net) المدرب على مجموعة بيانات أورام الدماغ (BraTS2020) ثم يقوم بتصنيف هذه المناطق على أنها أورام دبقية منخفضة الدرجة أو عالية الدرجة باستخدام نموذج آلة الدعم المتجه (SVM) استناداً إلى الميزات المستخرجة من الأقنعة المجزأة. في مجموعة الاختبار، حققت شبكة (U-Net) الخاصة بنا دقة قدرها 99,3%، بينما قدم مصنف (SVM) دقة إجمالية قدرها 93%.

الكلمات المفتاحية: أورام الدماغ، U-Net، SVM، MRI، BraTS، Segmentation.

Table of Contents

List of abbreviations	xi
List of Figures	xii
List of Tables	xiv
General Introduction	1
1 Deep Learning and Machine Learning	2
1.1 Introduction	2
1.2 What is Artificial Intelligence?	2
1.3 Machine Learning	3
1.3.1 Machine Learning approaches	4
1.3.1.1 Supervised Learning	4
1.3.1.2 Unsupervised Learning	4
1.3.1.3 Reinforcement Learning	5
1.3.2 Support Vector Machines (SVM)	5
1.4 Deep Learning	7
1.4.1 Convolutional Neural Networks (CNNs)	7
1.4.1.1 Convolutional Layer	8
1.4.1.2 Correction Layer (ReLU)	9
1.4.1.3 Pooling Layers	9
1.4.1.4 Fully Connected Layer	10
1.4.2 U-Net Architecture	10
1.4.2.1 Key Components of a U-Net Architecture	11

1.5	Magnetic Resonance Imaging (MRI)	12
1.6	Conclusion	13
2	State of the Art	14
2.1	Medical Imaging in Brain Tumor Diagnosis	14
2.2	The BraTS Dataset	17
2.3	Traditional Machine Learning Approaches	18
2.4	Deep Learning in Brain Tumor Segmentation	19
2.5	Tumor Classification Using Deep Features	20
2.6	Multiclass Tumor Region Segmentation	21
2.7	Challenges in the Field	21
3	Methodology and Contributions	24
3.1	Introduction	24
3.2	Proposed Framework Overview	25
3.2.1	End-to-End Inference Pipeline	25
3.2.2	Model Training Workflow	26
3.3	Dataset and Preprocessing	27
3.3.1	BraTS Dataset Description	27
3.3.2	Dataset Splitting	28
3.3.3	Data Preprocessing	29
3.4	Segmentation Module	30
3.4.1	U-Net Architecture	30
3.4.2	Evaluation Metrics for Segmentation	31
3.4.3	Segmentation Results	32
3.4.3.1	Accuracy	32
3.4.3.2	Loss	32
3.4.3.3	Dice Coefficient	33
3.4.3.4	Mean IoU	33
3.5	Classification Module	35
3.5.1	Feature Extraction	35
3.5.2	Feature Selection	36
3.5.3	SVM Model Training	36

3.5.4	Evaluation Metrics for Classification	36
3.5.5	Classification Results	37
3.6	Application Demo	38
3.6.1	Upload Page	38
3.6.2	Results Page	38
3.7	Conclusion	39
bibliography		42

List of abbreviations

AI Artificial Intelligence.

BraTS Brain Tumor Segmentation dataset.

CNN Convolutional Neural Network.

K-NN K-Nearest Neighbors.

ML Machine Learning.

MRI Magnetic Resonance Imaging.

RF Random Forest.

SVM Support Vector Machine.

U-Net U-Net Convolutional Neural Network.

List of Figures

1.1	Differences between AI, machine learning, and deep learning. [1]	3
1.2	Machine learning process.	3
1.3	Supervised learning process.	4
1.4	Unsupervised learning process.	4
1.5	Reinforcement learning process.	5
1.6	Support Vector Machine.	6
1.7	Deep learning process.	7
1.8	Convolutional Neural Network.	8
1.9	Convolution Layer.	9
1.10	U-Net Architecture.	11
1.11	Magnetic Resonance Imaging (MRI).	12
2.1	Example of T1-weighted MRI sequence.	15
2.2	Example of T1-weighted contrast-enhanced MRI sequence.	15
2.3	Example of T2-weighted MRI sequence.	16
2.4	Example of FLAIR MRI sequence.	16
3.1	Overview of the end-to-end inference pipeline.	25
3.2	Overview of the training workflow.	26
3.3	Brats modalities: T1, T1ce, T2, and T2-FLAIR.	27
3.4	Segmentation of Tumor classes.	28
3.5	Distribution of the training, validation, and test sets.	29
3.6	Segmentation accuracy over epochs.	32
3.7	Segmentation loss over epochs.	33
3.8	Segmentation Dice coefficient over epochs.	33

3.9	Segmentation mean IoU over epochs.	34
3.10	Example of segmentation results.	35
3.11	Confusion matrix for the SVM classifier.	37
3.12	Upload page of the application demo.	38
3.13	Results page of the application demo.	39

List of Tables

3.1	Segmentation performance on the test set	34
3.2	Classification report	37

General Introduction

Traditionally, radiologists rely on MRI scans to detect brain tumors, While this method is effective, it also has limitations analyzing hundreds of scans manually is time consuming and prone to human error. That is where technology comes in. With recent advances in artificial intelligence, especially deep learning, we now have powerful tools that can learn from medical images and help with faster and more accurate diagnosis.

In this project, we focus on building a hybrid system to detect brain tumors and determine whether they are low-grade or high-grade. We use a U-Net model for segmenting the tumor regions in MRI images. After identifying these regions, we extract important features and feed them into a Support Vector Machine (SVM) classifier to make the final prediction.

We use the BraTS2020 dataset, focusing on T2-weighted FLAIR images, to train and test our system. Our goal is to create a pipeline that is not only technically sound but also practical and helpful for medical professionals in real-world settings.

Chapter 1

Deep Learning and Machine Learning

1.1 Introduction

Artificial intelligence (AI) has become indispensable in medical imaging, offering tools that can assist—and in some cases outperform—radiologists in detecting and characterizing pathologies. In the context of brain tumors, AI-driven methods enable rapid and accurate identification of tumor boundaries and grading, directly impacting treatment planning and patient outcomes.

In this chapter,

1.2 What is Artificial Intelligence?

Artificial Intelligence (AI) is a multidisciplinary field focused on developing machines and computer programs capable of performing tasks that typically require human intelligence, such as visual perception, reasoning, decision making, and language understanding. According to [2], AI is defined as:

"the science and engineering of creating intelligent machines, particularly intelligent computer programs that can perform tasks requiring human intelligence, such as visual perception, decision making, and language translation."

In other words, AI includes both the study of human cognition—how people perceive,

learn, reason, and decide—and the development of algorithms and systems that can perform tasks requiring “intelligence,” such as visual recognition or decision making. While some AI techniques draw inspiration from biological processes (e.g. neural networks), the field also embraces purely mathematical and statistical methods.

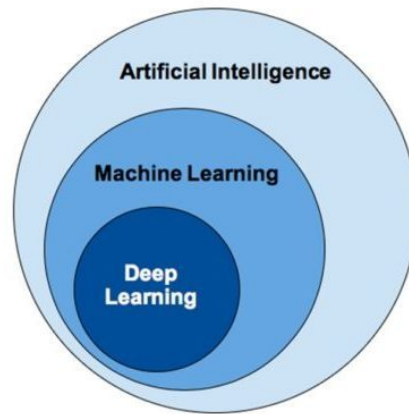


Figure 1.1: Differences between AI, machine learning, and deep learning. [1]

1.3 Machine Learning

Machine learning (ML) has emerged as a crucial area of study for organizations aiming to harness data resources and gain deeper insights into their operations. Unlike traditional programming methods, where explicit instructions are coded, machine learning enables systems to learn directly from data. In the medical imaging field, ML techniques offer powerful ways to analyze complex MRI data, supporting more accurate and efficient diagnostic processes. However, machine learning is a complex process that involves using diverse algorithms to iteratively learn from data, refine data representations, and make predictions. By feeding training data into these algorithms, increasingly accurate models can be developed. These machine learning models represent the knowledge acquired by algorithms during the training phase [3].

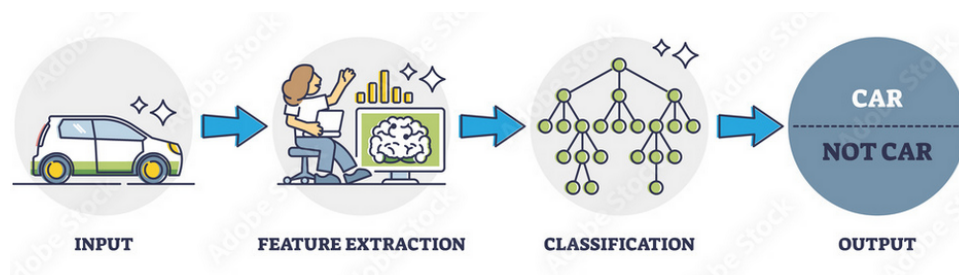


Figure 1.2: Machine learning process.

1.3.1 Machine Learning approaches

1.3.1.1 Supervised Learning

In supervised learning, the algorithm learns from labeled training data, where each data point is associated with a corresponding label or target value as depicted in Figure 1.3. Examples of supervised learning algorithms include linear regression , decision trees , random forests , support vector machines , and neural networks.

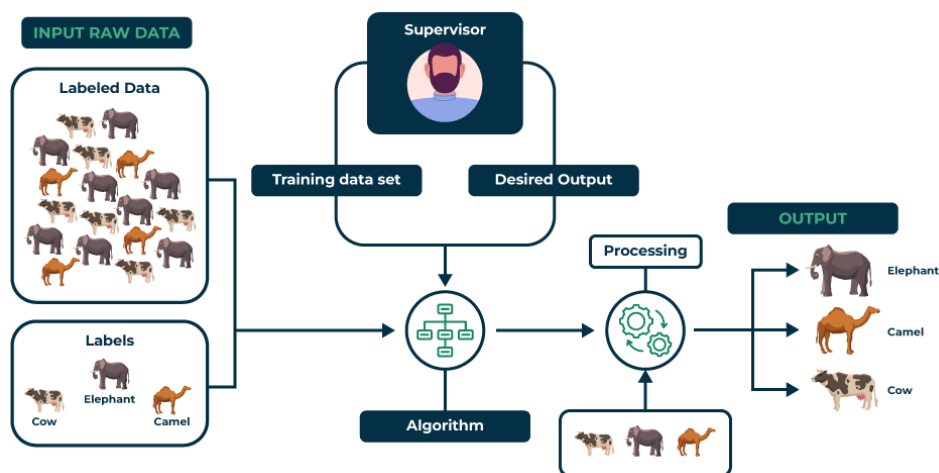


Figure 1.3: Supervised learning process.

1.3.1.2 Unsupervised Learning

Unsupervised learning deals with unlabeled data, where the algorithm learns to find patterns or structure in the data without any specific guidance. Such as k-means and hierarchical clustering, and dimensionality reduction techniques, such as principal component analysis and t-distributed stochastic neighbor embedding, Figure 1.4

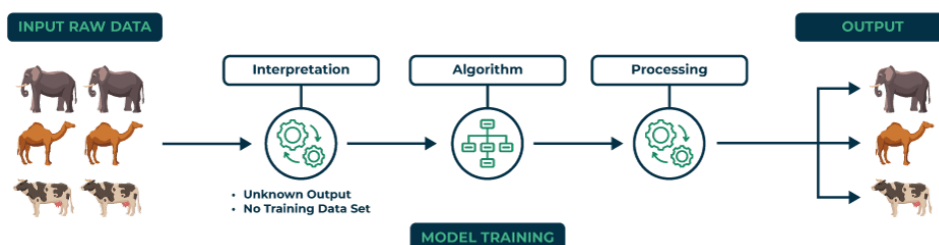


Figure 1.4: Unsupervised learning process.

1.3.1.3 Reinforcement Learning

Reinforcement learning is a type of machine learning where an agent learns to make decisions by interacting with an environment. The agent receives feedback in the form of rewards or penalties based on its actions, allowing it to learn optimal strategies over time. This approach is often used in robotics, game playing, and autonomous systems. Figure 1.5 illustrates the reinforcement learning process.

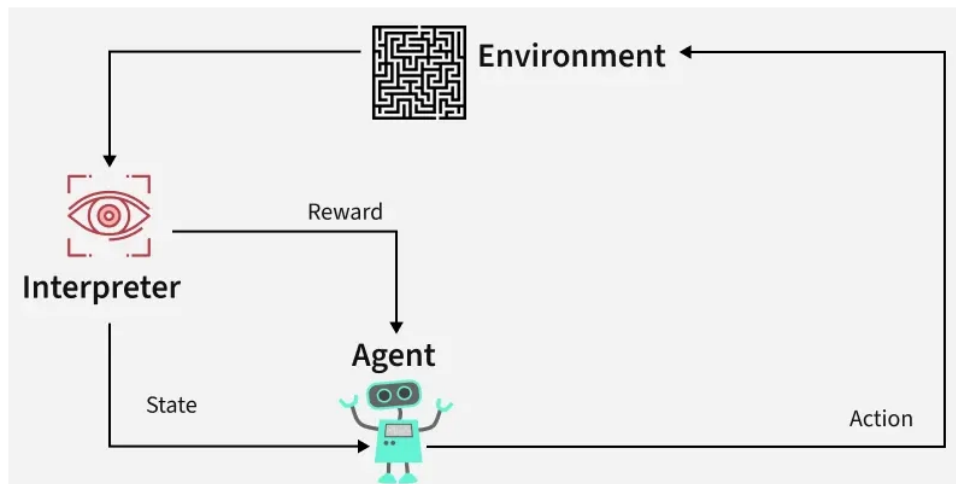


Figure 1.5: Reinforcement learning process.

1.3.2 Support Vector Machines (SVM)

Support Vector Machines (SVMs) are supervised machine learning models widely used for classification and regression tasks. The core idea of SVM is to find an optimal hyperplane that separates data points of different classes with the maximum possible margin, which enhances the model's ability to generalize to unseen data. SVMs can efficiently handle both linear and non-linear classification problems by employing the kernel trick, which implicitly maps input data into a higher-dimensional feature space where a linear separation becomes possible. The theoretical foundation of SVMs is based on the Structural Risk Minimization (SRM) principle, which aims to minimize an upper bound on the generalization error, offering advantages over traditional Empirical Risk Minimization approaches. Originally developed by Vapnik and colleagues in the 1990s, SVMs have become popular due to their strong empirical performance and robustness to overfitting, especially in high-dimensional spaces [4].

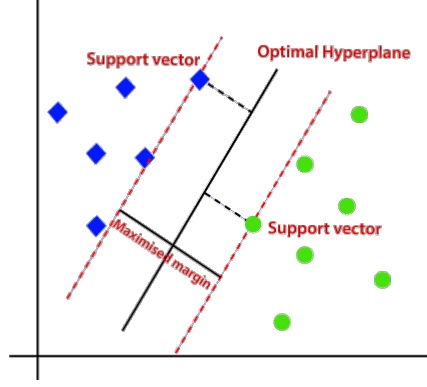


Figure 1.6: Support Vector Machine.

The fundamental formula defining the decision boundary of a Support Vector Machine (SVM) is a hyperplane expressed as:

$$\mathbf{w}^\top \mathbf{x} + b = 0 \quad (1.1)$$

where \mathbf{w} is the weight vector normal to the hyperplane, \mathbf{x} is the input feature vector, and b is the bias term.

For binary classification with labels $y_i \in \{+1, -1\}$, the SVM enforces the following constraints on each training point (\mathbf{x}_i, y_i) :

$$y_i(\mathbf{w}^\top \mathbf{x}_i + b) \geq 1, \quad \forall i. \quad (1.2)$$

The margin width (the distance between the closest points of each class to the hyperplane) is given by $\frac{2}{\|\mathbf{w}\|_2}$. Maximizing this margin is therefore equivalent to minimizing $\|\mathbf{w}\|_2$, leading to the following convex optimization problem:

$$\min_{\mathbf{w}, b} \quad \frac{1}{2} \|\mathbf{w}\|_2^2, \quad (1.3)$$

$$\text{subject to} \quad y_i(\mathbf{w}^\top \mathbf{x}_i + b) \geq 1, \quad \forall i. \quad (1.4)$$

For non-linearly separable data, slack variables and kernel functions can be introduced, but the core formulation remains centered on maximizing the margin around this hyperplane.

1.4 Deep Learning

Deep learning has emerged as a powerful approach for modeling complex data through intricate architectures that incorporate non-linear transformations. Neural networks, including deep neural networks, serve as the fundamental components of deep learning. These techniques have achieved remarkable progress in various domains such as sound and image processing, enabling tasks like facial recognition, speech recognition, computer vision, language processing, and text classification. The potential applications of deep learning are vast and continue to expand.

Different types of neural network architectures, such as multilayer perceptrons, Convolutional Neural Networks (CNNs), and recurrent neural networks, cater to specific data types and tasks. These architectures are characterized by deep layers organized in a cascading manner. Successful implementation of deep learning requires well-designed stochastic optimization algorithms, appropriate initialization techniques, and thoughtful structure selection.

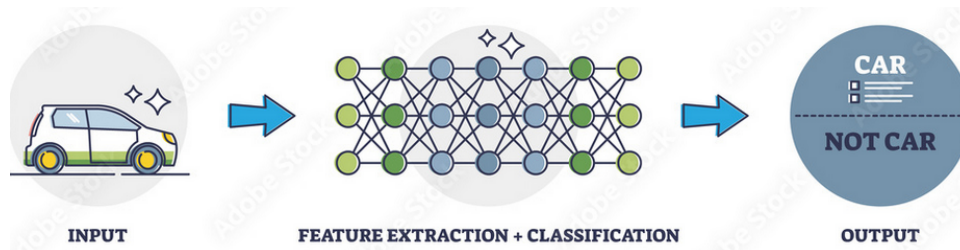


Figure 1.7: Deep learning process.

1.4.1 Convolutional Neural Networks (CNNs)

A convolutional neural network (CNN) is a type of neural network with a topology similar to a grid, inspired by the human brain. It is commonly used for image processing tasks, as well as natural language processing.

A CNN consists of two main parts. The input is an image, represented as a 2D matrix of pixels for grayscale images and a 3D matrix of pixels for color images (Red, Green, Blue).

The first part of a CNN is the convolutional layer, which acts as a feature extractor. The image is passed through a series of filters, or convolution kernels, to generate new images called feature maps. Some intermediate filters reduce the image resolution. Finally, the feature maps are concatenated to form a vector of features, known as the CNN code.

The output of the convolutional layer, the CNN code, is the input to the second part of the network. The main role of this part is to combine the features of the CNN code to classify the image. The output is a final layer with one neuron per category.

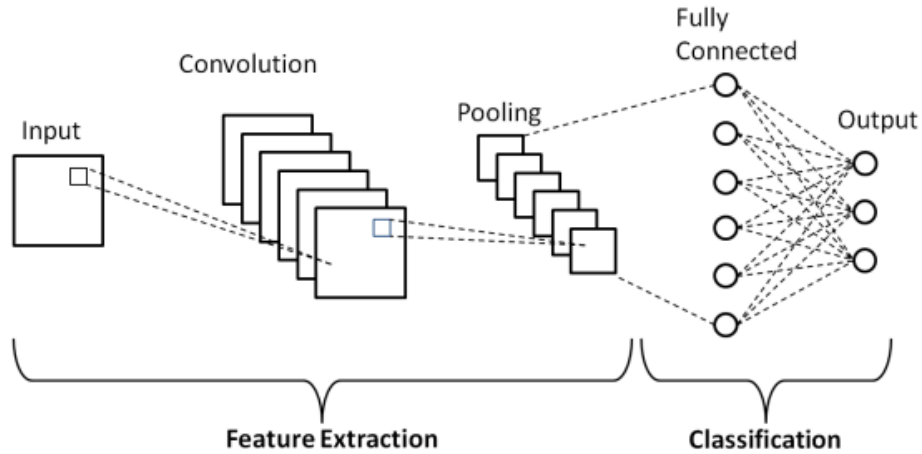


Figure 1.8: Convolutional Neural Network.

1.4.1.1 Convolutional Layer

The convolutional layer is the most important layer and usually the first layer in a CNN. It consists of three main elements involved in the convolution operation:

- **Input image** (f)
- **Feature detector (filter)** (h)
- **Feature map (output)** (G)

A convolution takes an image and a filter as input and applies the convolution operation to produce a new image, called the activation map or feature map.

The activation map values are calculated using the following formula:

$$G[m,n] = (f * h)[m,n] \quad (1.5)$$

where

- f is the input image,
- h is the convolution filter,

- m, n are the spatial indices over which the convolution is computed.

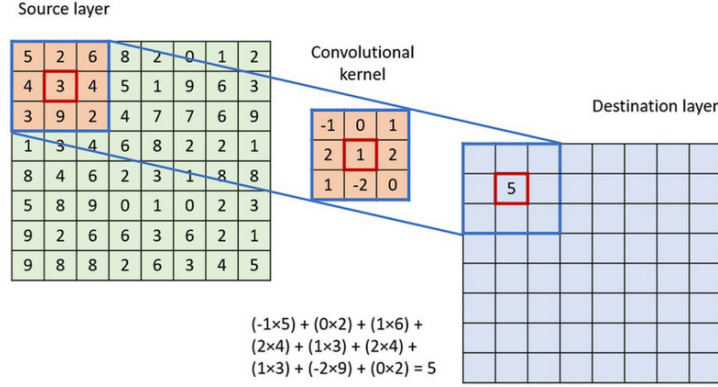


Figure 1.9: Convolution Layer.

1.4.1.2 Correction Layer (ReLU)

The Correction Layer, typically implemented using the Rectified Linear Unit (ReLU), is an activation function applied after each convolution operation to enhance processing efficiency. It replaces all negative pixel values with zero, introducing non-linearity into the network while maintaining computational simplicity. The ReLU function is defined as:

$$f(x) = \max(0, x) \quad (1.6)$$

Several other activation functions exist, such as the sigmoid function, the hyperbolic tangent function (tanh), and the hyperbolic saturating tangent function. However, ReLU is often preferred in deep learning models because it enables faster convergence and better performance compared to these alternatives.

1.4.1.3 Pooling Layers

Pooling layers are utilized to reduce the spatial dimensions of feature maps while preserving the most important information and features. This helps decrease computational complexity and mitigate overfitting. There are several types of pooling operations:

- **Max Pooling:** It selects the maximum value from each patch of the feature map. Typically, a 2×2 patch is used. Max pooling is the most commonly used pooling method.
- **Min Pooling:** The inverse of max pooling; it selects the minimum value from each patch

of the feature map.

- **Average Pooling:** It computes the average of all the values within each patch of the feature map by summing the values and dividing by the number of elements.
- **Sum Pooling:** It computes the sum of all elements within each patch of the feature map.
- **Flattening:** After the pooling operations, the resulting feature maps are flattened into a single one-dimensional vector to prepare for fully connected (dense) layers.

1.4.1.4 Fully Connected Layer

after the convolution and pooling layers, the high-level reasoning in the neural network is done in fully connected layers. The output of flattening is the input of FC layers which are the same as artificial neural networks and carry out the same mathematical operations. The last fully-connected layer uses an activation function such as sigmoid or softmax to get probabilities of the outputs.

1.4.2 U-Net Architecture

U-Net is a convolutional neural network architecture specifically designed for biomedical image segmentation. Introduced by Ronneberger et al. in 2015, U-Net features a symmetric encoder-decoder structure: the contracting path (encoder) captures image context through successive convolution and pooling operations, while the expansive path (decoder) enables precise localization via upsampling and concatenation with high-resolution features from the encoder. This architecture allows U-Net to achieve accurate segmentation even with limited annotated data by leveraging extensive data augmentation. U-Net has demonstrated superior performance in various biomedical segmentation challenges, notably outperforming previous methods in tasks such as neuronal structure segmentation in electron microscopy images and cell tracking in light microscopy [5].

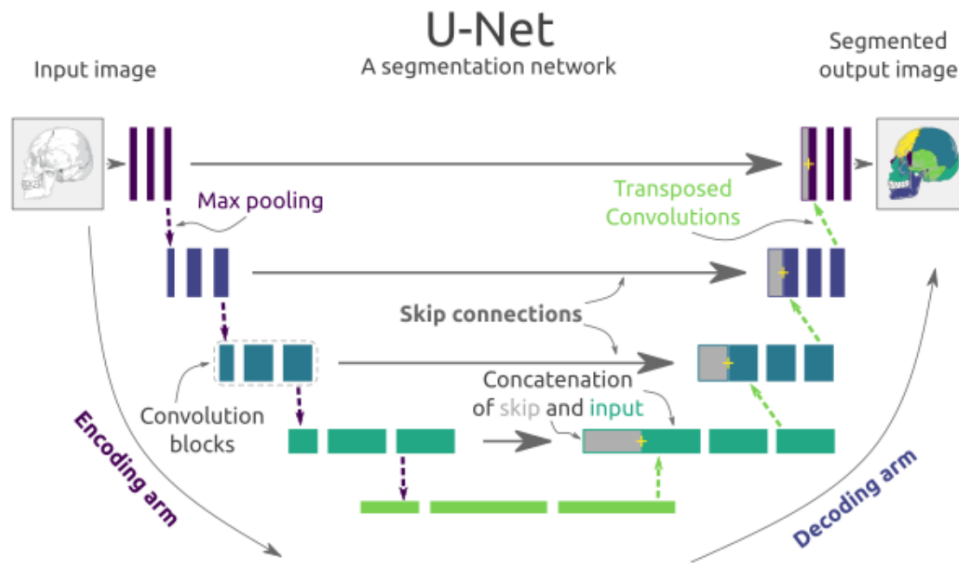


Figure 1.10: U-Net Architecture.

1.4.2.1 Key Components of a U-Net Architecture

- **Contracting Path (Encoder):**

This path is responsible for extracting contextual features from the input image. It consists of repeated blocks of two 3×3 convolutional layers (with ReLU activation), followed by a 2×2 max pooling operation for downsampling. With each downsampling step, the number of feature channels is doubled, allowing the network to capture increasingly abstract representations of the input.

- **Bottleneck:**

Located at the deepest part of the network, the bottleneck consists of convolutional layers without pooling. It serves as the bridge between the encoder and decoder, capturing the most condensed and abstract features of the input.

- **Expansive Path (Decoder):**

This path reconstructs the spatial resolution of the feature maps and enables precise localization. Each step in the decoder involves upsampling the feature map (often via transposed convolution or up-convolution), concatenating it with the corresponding feature map from the encoder (skip connection), and then applying two 3×3 convolutions (with ReLU activation). The number of feature channels is halved at each upsampling step.

- **Skip Connections:**

At each level, feature maps from the encoder are concatenated with the upsampled feature maps in the decoder. These skip connections help retain high-resolution spatial information that might otherwise be lost during downsampling, improving the accuracy of segmentation boundaries.

- **Final Output Layer:**

The last layer is typically a 1×1 convolution that maps each feature vector to the desired number of output classes, producing a pixel-wise classification map for segmentation tasks.

This U-shaped design enables U-Net to effectively combine global context with fine-grained localization, making it highly effective for precise image segmentation tasks.

1.5 Megnatic Resonance Imaging (MRI)

Magnetic resonance imaging (MRI) uses a powerful magnetic field and radio waves to generate detailed and high-resolution images of organs and tissues inside the human body, as depicted in Figure 1.11. This non-invasive imaging method offers significant advantages in visualizing intricate details of the brain, spinal cord, joints, and soft tissues. MRI plays a vital role in diagnosing and evaluating a wide range of medical conditions, such as tumors, neurological disorders, and musculoskeletal injuries. Its ability to produce precise and detailed images aids healthcare professionals in accurately identifying and assessing these conditions, enabling effective treatment planning and optimal patient care [6].

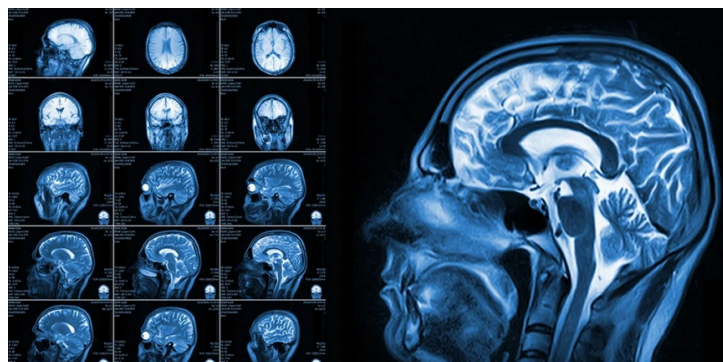


Figure 1.11: Magnetic Resonance Imaging (MRI).

1.6 Conclusion

In this chapter, we established the theoretical foundation necessary for our study on brain tumor analysis using artificial intelligence techniques. We first explored the fundamental concepts of artificial intelligence, machine learning, and deep learning, emphasizing their significance in the medical imaging domain. We discussed the various machine learning approaches, highlighting the principles and applications of Support Vector Machines (SVMs) for classification tasks. Furthermore, we introduced deep learning methodologies, focusing on Convolutional Neural Networks (CNNs) and their components, including convolutional, pooling, and fully connected layers. Finally, we presented the U-Net architecture, a specialized CNN model for biomedical image segmentation, which plays a crucial role in the segmentation phase of our proposed hybrid approach. This theoretical background sets the stage for the practical implementation and evaluation of our models in the following chapters.

Chapter 2

State of the Art

2.1 Medical Imaging in Brain Tumor Diagnosis

Magnetic Resonance Imaging (MRI) has emerged as the gold standard for brain tumor diagnosis due to its superior soft tissue contrast, high spatial resolution, and non-invasive nature [7]. Unlike other imaging modalities such as CT scans, MRI provides detailed structural information without exposing patients to ionizing radiation, making it particularly valuable for serial monitoring and treatment planning [8].

The multimodal nature of MRI is especially useful in brain tumor assessment, with each sequence highlighting different aspects of the tumor [9]:

- **T1-weighted (T1):** Provides excellent anatomical detail and clearly delineates boundaries between gray and white matter. Tumors typically appear hypointense (darker) compared to surrounding tissue.

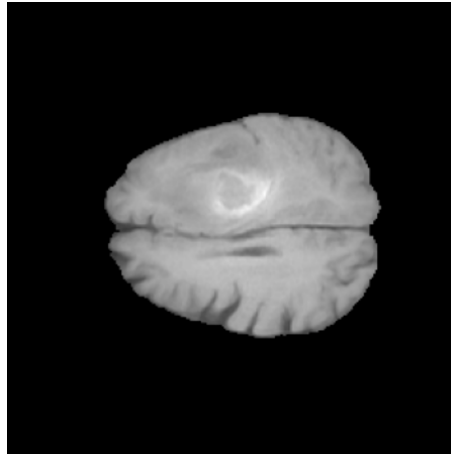


Figure 2.1: Example of T1-weighted MRI sequence.

- **T1 with contrast enhancement (T1ce):** After gadolinium administration, areas with disrupted blood-brain barrier (characteristic of high-grade tumors) enhance, appearing hyperintense and revealing the active tumor core.

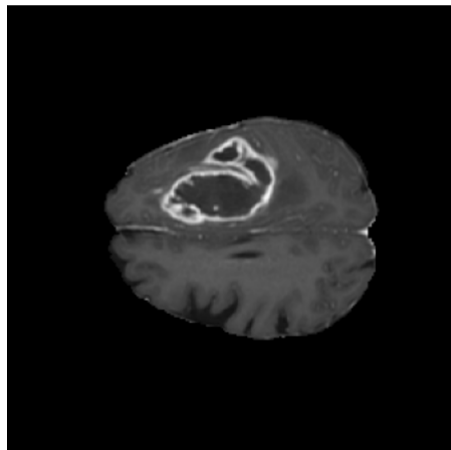


Figure 2.2: Example of T1-weighted contrast-enhanced MRI sequence.

- **T2-weighted (T2):** Highlights areas with increased water content, making it valuable for identifying edema and infiltrative tumor components. Tumors and surrounding edema appear hyperintense.

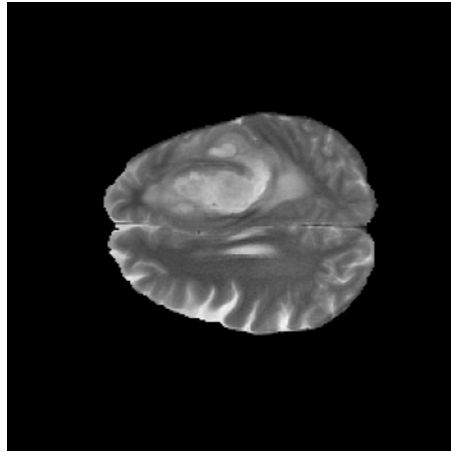


Figure 2.3: Example of T2-weighted MRI sequence.

- **Fluid-Attenuated Inversion Recovery (FLAIR):** Suppresses cerebrospinal fluid signals, enhancing the visibility of periventricular lesions and edema associated with tumors.

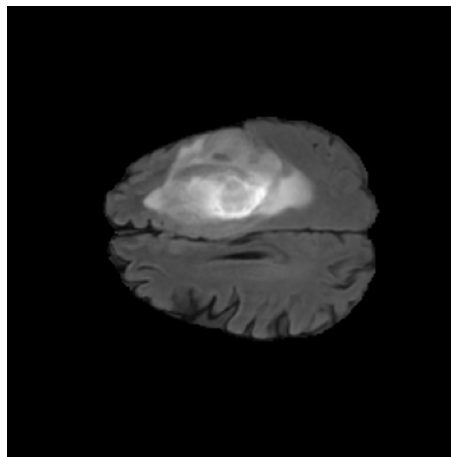


Figure 2.4: Example of FLAIR MRI sequence.

Traditionally, neuroradiologists diagnose brain tumors by visually inspecting these multiple MRI sequences, mentally integrating information across modalities to determine tumor boundaries, assess grade, and identify critical structures [10]. This process is inherently subjective, time-consuming, and susceptible to inter-observer variability, with studies reporting considerable disagreement even among experienced radiologists. These limitations have driven significant interest in developing computational approaches for automated and semi-automated tumor analysis.

2.2 The BraTS Dataset

The Brain Tumor Segmentation (BraTS) challenge and dataset represent a landmark initiative in standardizing the evaluation of brain tumor segmentation algorithms [8, 9]. Since its inception in 2012, BraTS has evolved into the most widely adopted benchmark for algorithm development and performance assessment in this domain [11].

The BraTS dataset is particularly valuable due to its:

- **Multimodal approach:** Each case includes four co-registered MRI sequences (T1, T1ce, T2, and FLAIR), enabling algorithms to leverage complementary information [12].
- **Standardized preprocessing:** All images undergo skull-stripping, resampling to isotropic 1mm³ voxels, and registration to a common anatomical template, reducing technical variability [9].
- **Expert annotations:** Each tumor is manually segmented by experienced neuroradiologists following a standardized protocol, with additional verification to ensure quality [8].
- **Multi-institutional data:** Images are acquired from multiple institutions using different scanners and protocols, promoting the development of robust algorithms [11].

1. **Enhancing Tumor (ET):** Areas showing hyperintensity in T1ce relative to T1
2. **Tumor Core (TC):** Encompassing the ET, necrotic components, and non-enhancing tumor
3. **Whole Tumor (WT):** Including all tumor tissues and surrounding edema

This hierarchical annotation structure enables the evaluation of algorithms at multiple levels of detail, from gross tumor detection to fine-grained sub-region delineation [9]. The BraTS datasets and associated challenges have catalyzed significant methodological advances, with performance metrics improving consistently year over year [13].

2.3 Traditional Machine Learning Approaches

Before the deep learning revolution, brain tumor segmentation and classification relied heavily on traditional machine learning techniques coupled with handcrafted feature extraction [14]. These approaches typically followed a pipeline of preprocessing, feature extraction, and classification using conventional machine learning algorithms.

Support Vector Machines (SVM) were particularly popular for brain tumor classification and segmentation due to their strong theoretical foundations and effectiveness with high-dimensional data [15]. Zacharaki et al. [16] developed an SVM-based system that extracted 161 features including intensity, texture, and shape characteristics from multi-parametric MRI, achieving 85% accuracy in discriminating between different tumor types. Similarly, Reza and Iftekharuddin [17] combined texture features with fractal analysis and SVM classification to segment brain tumors, demonstrating competitive performance on earlier BraTS datasets.

Random Forest (RF) classifiers also showed promise due to their robustness to overfitting and ability to handle multi-class problems efficiently. Zikic et al. [18] employed RF with context-aware features for brain tumor segmentation, while Festa et al. [19] achieved strong results in the BraTS 2013 challenge using RF with handcrafted features. Tustison et al. [20] further refined this approach by incorporating an extensive feature set derived from multiple MRI sequences, winning the BraTS 2013 challenge.

K-Nearest Neighbors (K-NN) algorithms were explored by Simi and Joseph [21], who combined texture features with k-NN classification for tumor segmentation. Huang et al. [22] also investigated k-NN for brain tumor classification using multispectral MRI features.

Despite their success, these traditional approaches faced significant limitations:

- **Dependence on handcrafted features:** Their performance was heavily contingent on the quality of manually designed features, requiring substantial domain expertise [23].
- **Limited contextual understanding:** Most methods struggled to incorporate broader spatial context, often relying on voxel-wise or small-patch features [24].
- **Computational inefficiency:** Sequential processing of feature extraction followed by classification led to lengthy processing times impractical for clinical settings [25].

- **Suboptimal performance on heterogeneous tumors:** The high variability in tumor appearance often challenged these methods, particularly for complex or atypical cases [8].

These limitations ultimately paved the way for the adoption of deep learning techniques, which could learn hierarchical features directly from data and better capture the complex patterns present in brain tumor images.

2.4 Deep Learning in Brain Tumor Segmentation

The adoption of deep learning, particularly Convolutional Neural Networks (CNN), has revolutionized brain tumor segmentation by enabling automatic hierarchical feature learning directly from imaging data [24]. This paradigm shift has eliminated the need for handcrafted features, and led to improving segmentation accuracy and robustness.

Among deep learning architectures, U-Net has emerged as the cornerstone for medical image segmentation, including brain tumor analysis [26]. Its distinctive encoder-decoder structure with skip connections effectively combines localization and contextual information, preserving fine details while capturing broader tumor patterns. Urban et al. [27] were among the first to apply CNNs to brain tumor segmentation, while Pereira et al. [28] demonstrated that carefully designed CNN architectures could outperform traditional methods on the BraTS challenge.

Several U-Net variants have been developed specifically for brain tumor segmentation:

- **3D U-Net:** Çiçek et al. [29] extended the original 2D architecture to process volumetric data, better capturing the three-dimensional nature of tumors. Isensee et al. [30] further refined this approach, achieving top ranking in the BraTS 2018 challenge with a 3D U-Net variant.
- **U-Net++:** Zhou et al. [31] proposed a nested architecture with redesigned skip pathways to bridge the semantic gap between encoder and decoder features. Experimental results showed improved performance on several medical segmentation tasks, including brain tumors.
- **Attention U-Net:** Oktay et al. [32] incorporated attention gates to highlight relevant

features and suppress irrelevant regions, improving segmentation accuracy particularly at tumor boundaries. Schlemper et al. [33] demonstrated the effectiveness of this approach for multi-class tumor segmentation.

The performance of these deep learning models on BraTS challenges has improved consistently over time. In BraTS 2018, Myronenko [34] achieved exceptional results with an encoder-decoder architecture incorporating variational components. McKinley et al. [35] further advanced the field with an ensemble of 3D U-Nets, achieving Dice scores of 0.91, 0.83, and 0.78 for whole tumor, tumor core, and enhancing tumor, respectively. The BraTS 2020 challenge saw even more impressive results, with top-performing methods consistently achieving Dice scores above 0.90 for whole tumor segmentation [13].

Despite these advancements, challenges remain in achieving clinically acceptable performance across diverse patient populations and imaging protocols, driving continuous innovation in the field.

2.5 Tumor Classification Using Deep Features

While segmentation delineates tumor boundaries, classification determines tumor type and characteristics—a critical aspect of diagnosis and treatment planning. Modern approaches increasingly leverage deep features, either independently or in conjunction with traditional machine learning classifiers like Support Vector Machines (SVMs).

Pretrained Convolutional Neural Networks (CNNs) have proven extremely effective as feature extractors for brain tumor classification. Afshar et al. [36] employed a modified ResNet architecture to extract deep features from brain MRI, achieving 93.68% accuracy in classifying tumors into different grades. Similarly, Deepak and Ameer [37] utilized DenseNet for feature extraction followed by SVM classification, reporting improved performance compared to traditional methods. Sajjad et al. [38] extended this approach by fine-tuning VGG-19 on brain tumor images, extracting features from intermediate layers for subsequent classification.

2.6 Multiclass Tumor Region Segmentation

Accurate delineation of different tumor sub-regions represents one of the most challenging aspects of brain tumor analysis, requiring discrimination between biologically distinct components that may appear visually similar [9]. The BraTS challenge specifically evaluates algorithms on their ability to segment three tumor sub-components: Enhancing Tumor (ET), Tumor Core (TC), and Whole Tumor (WT).

Multi-class tumor segmentation approaches have evolved significantly in recent years. Zhao et al. [39] proposed a multi-scale CNN architecture specifically designed to address the hierarchical nature of tumor sub-regions, achieving meaningful improvements in enhancing tumor segmentation. Wang et al. [40] developed a cascaded approach where initial whole tumor segmentation guided subsequent sub-region delineation, reducing false positives in non-tumor regions. Kamnitsas et al. [41] introduced DeepMedic, a dual-pathway 3D CNN architecture that simultaneously processed input at different resolutions, effectively capturing both fine details and broader contextual information.

The continued advancement of multi-class tumor segmentation approaches promises to improve diagnostic accuracy and treatment planning by providing more detailed characterization of tumor heterogeneity.

2.7 Challenges in the Field

Despite the significant progress, several persistent challenges continue to impact the development and clinical translation of automated brain tumor analysis systems.

Class imbalance remains a fundamental issue in both segmentation and classification tasks. Brain tumors typically occupy less than 1% of the total brain volume, creating extreme imbalance that can bias models toward the majority (healthy tissue) class [28]. While techniques such as patch-based training [24], specialized loss functions [30], and data augmentation [42] have partially addressed this issue, performance on smaller tumor sub-regions (particularly enhancing tumor) continues to lag behind whole tumor segmentation.

The **interpretability of deep models** presents another significant hurdle, particularly for clinical adoption. The "black box" nature of deep learning approaches creates reluctance among

clinicians to trust automated segmentations without understanding the underlying decision process [43]. Recent work by Natekar et al. [44] has explored visualization techniques to highlight features influencing segmentation decisions, while Lucieri et al. [45] demonstrated the value of attention maps for explaining tumor classification outcomes. However, creating truly interpretable deep learning systems remains an open challenge.

Generalization across different MRI scanners and patients continues to limit clinical applicability. Models trained on specific datasets often experience performance degradation when applied to images acquired with different hardware, field strengths, or acquisition parameters [8]. Zech et al. [46] documented this domain shift problem in medical imaging, while Kamnitsas et al. [41] proposed domain adaptation techniques to mitigate its effects. More recently, Shaw et al. [47] explored adversarial domain adaptation specifically for brain tumor segmentation, showing promising results in cross-scanner generalization.

The **lack of labeled data** remains a fundamental limitation, particularly for rare tumor types or unusual presentations. While the BraTS dataset has grown substantially, it still represents a fraction of the true biological variability of brain tumors [11]. Semi-supervised approaches by Sedai et al. [48] leverage unlabeled data to improve generalization, while Zhao et al. [49] demonstrated promising results with data-efficient few-shot learning techniques. Transfer learning approaches by Ghafoorian et al. [50] have also shown potential in adapting pre-trained models to limited target datasets.

Additional challenges include:

- **Computational efficiency:** 3D deep learning models often require substantial computational resources beyond what's available in many clinical settings [41].
- **Longitudinal analysis:** Most current approaches treat each time point independently, missing the opportunity to leverage temporal information in patient monitoring [51].
- **Integration with other data types:** Combining imaging with clinical, genomic, and pathological data remains challenging despite its potential to improve diagnostic accuracy [11].
- **Clinically relevant evaluation metrics:** Standard technical metrics like Dice coefficients may not directly translate to clinical utility, creating a disconnect between research

advances and clinical impact [52].

Addressing these challenges will require multidisciplinary collaboration between computer scientists, medical imaging experts, and clinicians to develop solutions that are not only technically sophisticated but also clinically relevant and practically deployable.

Chapter 3

Methodology and Contributions

3.1 Introduction

In this chapter, we present the core contributions of our work on automated brain tumor detection in magnetic resonance (MR) images. Building upon the BraTS benchmark dataset [8], our pipeline integrates a deep learning–based segmentation module with a classical machine learning classifier and culminates in a user-friendly demo application. The main objectives of this chapter are:

- To describe a tailored U-Net–based segmentation pipeline for delineating tumor subregions in MRI slices.
- To detail a feature-extraction and SVM classification scheme that distinguishes high-grade from low-grade gliomas using volumetric, intensity, texture, and shape descriptors.
- To demonstrate the integration of these modules within an end-to-end application for streamlined inference on new patient data.

The remainder of this chapter is organized as follows. In Section 3.3, we introduce the dataset and preprocessing steps. Section 3.4 details the U-Net segmentation module, including architecture and training protocol. Section 3.5 covers the feature engineering and SVM classification. Section 3.6 presents the design and functionality of our demo application. We conclude with a discussion of key findings and future directions.

3.2 Proposed Framework Overview

In this section, we look at our proposed framework from a systematic perspective. The framework is designed to perform end-to-end brain tumor segmentation and classification. We will discuss the design of the final pipeline and the training workflow to achieve the desired results.

3.2.1 End-to-End Inference Pipeline

The purpose of our project is to have an end-to-end inference pipeline accepts a raw MR image as input, applies preprocessing steps, performs segmentation of the tumor region using the trained U-Net model, classifies the tumor grade via the SVM classifier, and finally outputs the original image overlaid with the segmentation mask along with the predicted grade.

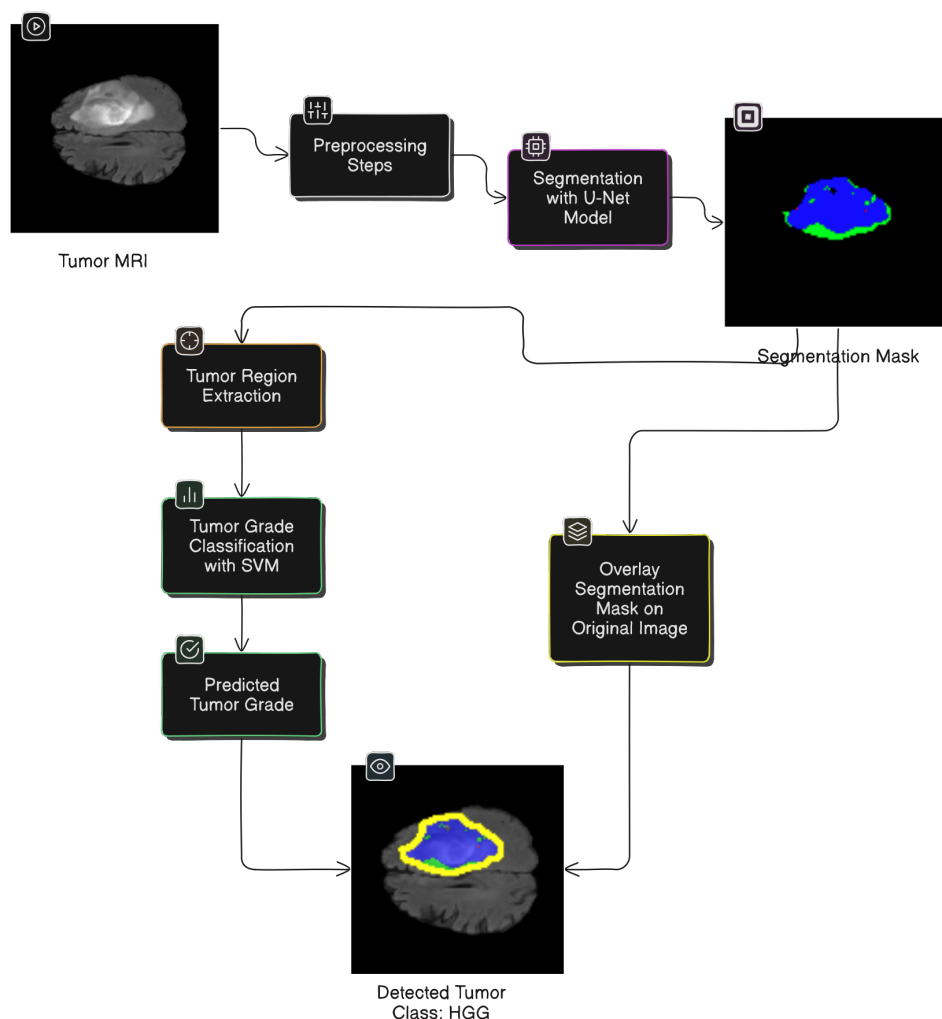


Figure 3.1: Overview of the end-to-end inference pipeline.

3.2.2 Model Training Workflow

The training workflow begins with the BraTS dataset. After preprocessing and augmentation, the data is split into training, validation, and test sets. We then train the U-Net segmentation model in parallel with feature extraction followed by SVM classifier training, yielding two standalone models for inference.

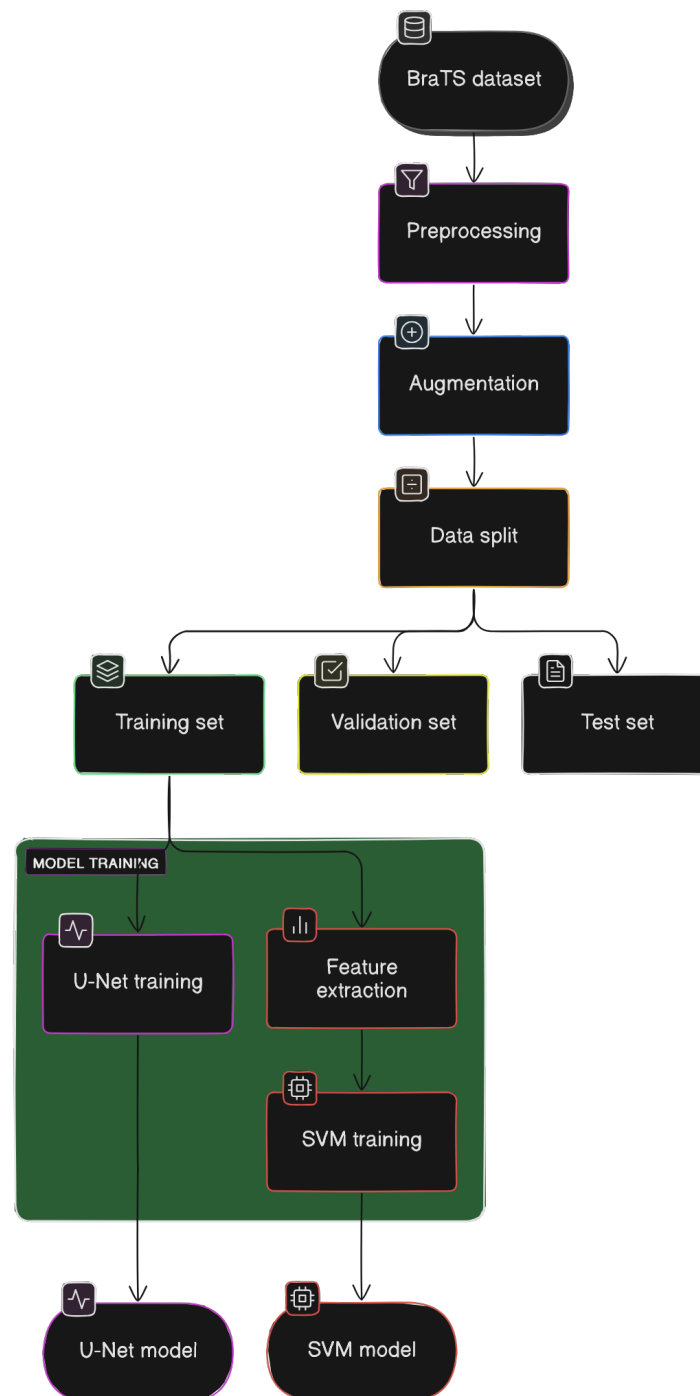


Figure 3.2: Overview of the training workflow.

3.3 Dataset and Preprocessing

In order to train our hybrid model we used the Brain Tumor Segmentation (BraTS) 2020 dataset, which is a collection of multimodal Magnetic Resonance Imaging (MRI) scans used for the segmentation of brain tumors.

3.3.1 BraTS Dataset Description

The dataset includes MRI scans from glioma patients, providing four different MRI modalities per patient:

1. **Native (T1)**
2. **Post-contrast T1-weighted (T1ce - contrast enhanced)**
3. **T2-weighted (T2)**
4. **T2-FLAIR (T2 - Fluid Attenuated Inversion Recovery)**
5. **Tumor Segmentation Mask**

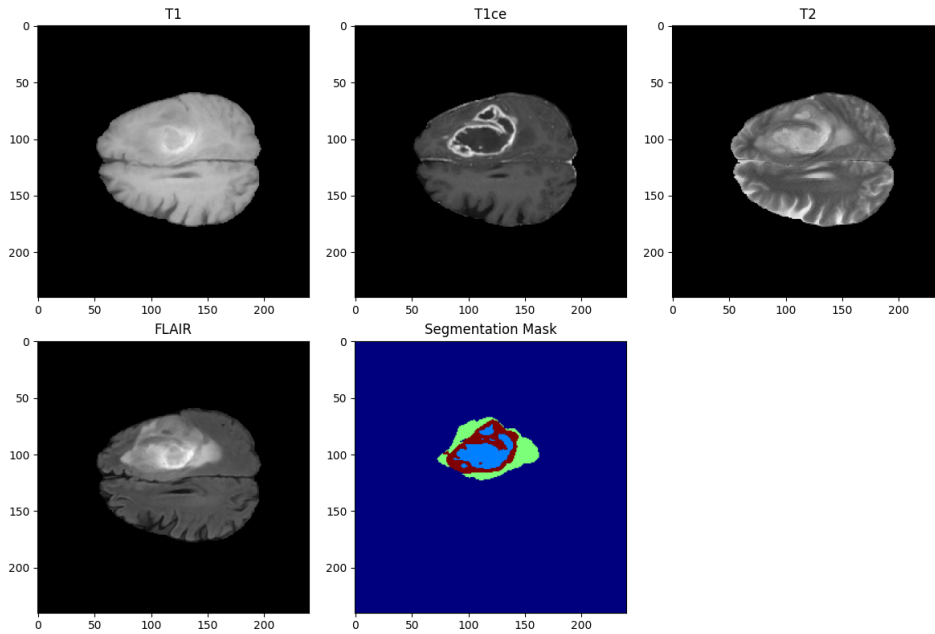


Figure 3.3: Brats modalities: T1, T1ce, T2, and T2-FLAIR.

These scans come with expert-annotated segmentation masks that delineate the tumor into various sub-regions, such as the necrotic and non-enhancing tumor core, the peritumoral edema,

and the enhancing tumor. Research has demonstrated that accurate segmentation is linked to improved prognostic assessments and treatment outcomes.

- **Class 0 (Not Tumor):** This class represents normal brain tissue or background, where no tumor tissue is present.
- **Class 1 (Non-Enhancing Tumor):** This class corresponds to the necrotic or non-enhancing core regions of the tumor. These areas typically lack contrast enhancement and may include dead or less active tumor tissue.
- **Class 2 (Edema):** This class identifies regions of peritumoral edema, which is the swelling around the tumor caused by fluid accumulation. Edema is important for understanding the extent of the tumor's impact on surrounding brain tissue.
- **Class 4 (Enhancing Tumor):** This class captures the actively enhancing parts of the tumor, visible after the administration of a contrast agent. These regions often indicate aggressive tumor tissue with increased blood flow and permeability.

To visually interpret these segmentations, we map the categorical labels to a custom colormap. In our example, we use four distinct colors to represent:

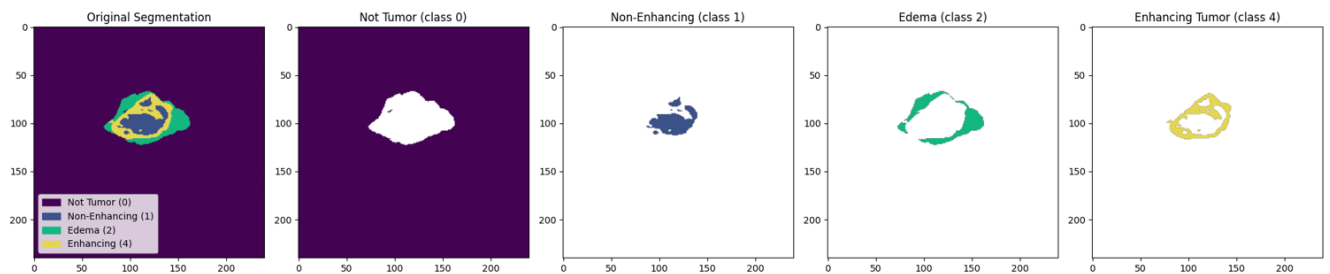


Figure 3.4: Segmentation of Tumor classes.

3.3.2 Dataset Splitting

To train and evaluate our model effectively, we need to partition our dataset into three subsets:

- **Training Set (70%):** Used to learn the model parameters.
- **Validation Set (approximately 20%):** Used for tuning hyperparameters and preventing overfitting.

- **Test Set (10%):** Used for assessing the final model’s performance on unseen data.

This split can be done randomly or in a stratified manner (to preserve the class distribution), which is especially useful when dealing with imbalanced datasets. Properly splitting the dataset is crucial for building a robust model that generalizes well to new data.

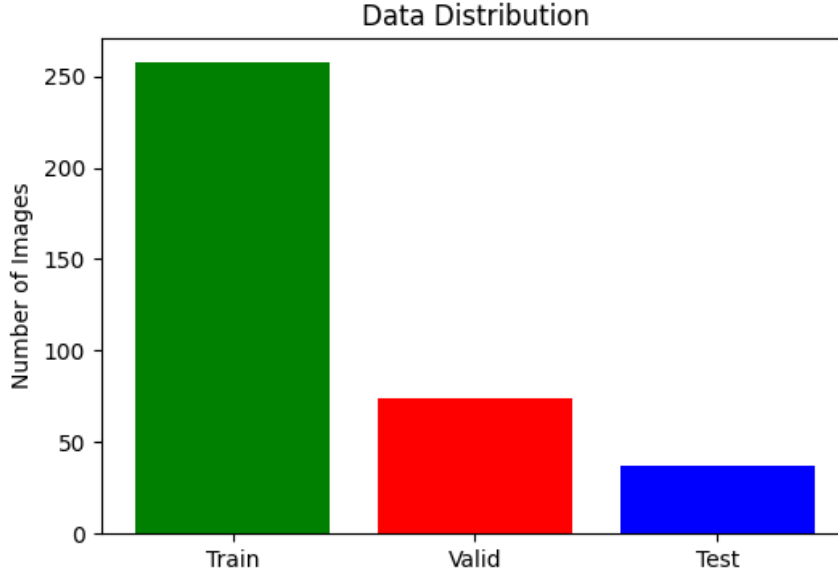


Figure 3.5: Distribution of the training, validation, and test sets.

3.3.3 Data Preprocessing

Before feeding MR volumes into our models, we apply a series of standardized preprocessing steps to ensure consistency and improve model robustness. Our pipeline operates on 2D axial slices extracted from 3D volumes, as follows:

1. **Slice Extraction.** For each patient volume, we select 100 consecutive axial slices starting at index 22. This avoids initial and final slices that contain little anatomical information.
2. **Resizing.**
 - *Image Slices:* Each extracted slice is resized to 128×128 pixels to match the U-Net input dimensions.
 - *Segmentation Masks:* Corresponding ground-truth masks are first resized to 240×240 (to preserve label fidelity) and later downsampled alongside images during one-hot

encoding.

3. **Intensity Normalization.** All pixel intensities in a slice are divided by the global maximum value of that volume, scaling inputs to the $[0, 1]$ range. This step harmonizes contrast across patients and modalities.
4. **Augmentation.** To increase effective training diversity, random geometric transformations are applied during batch generation:
 - Horizontal and vertical flips (each with 50% probability).
 - Rotations by multiples of 90° (randomly chosen among $0^\circ, 90^\circ, 180^\circ, 270^\circ$).

These preprocessing routines standardize input dimensions, normalize intensity distributions, and inject variability—laying a solid foundation for both segmentation and classification tasks.

3.4 Segmentation Module

The segmentation module is responsible for delineating tumor subregions in MR slices. It consists of a U-Net–based convolutional network for mask prediction.

3.4.1 U-Net Architecture

Our U-Net follows the standard encoder–decoder pattern with skip connections:

- **Encoder:** Four downsampling blocks, each with two Conv2D layers (kernel size 3×3 , ReLU activation) followed by MaxPooling2D.
- **Bottleneck:** Two Conv2D layers at the lowest resolution, with a dropout of 0.2 to reduce overfitting.
- **Decoder:** Four upsampling blocks, each using UpSampling2D + Conv2D (2×2) and concatenation with the corresponding encoder feature map.
- **Output:** A final Conv2D layer with a 1×1 kernel and softmax activation to produce a four-channel segmentation mask.

3.4.2 Evaluation Metrics for Segmentation

In segmentation tasks, *accuracy* measures the overall proportion of correctly classified pixels. However, in datasets like BraTS2020—where the background (non-tumor) pixels vastly outnumber tumor pixels—accuracy can be misleading. Therefore, we employ the following metrics for a more balanced evaluation:

- **Precision** (Positive Predictive Value) Measures the fraction of predicted tumor pixels that are truly tumor:

$$\text{Precision} = \frac{\text{TP}}{\text{TP} + \text{FP}}$$

where

- TP = number of true positive pixels,
- FP = number of false positive pixels.

- **Sensitivity** (Recall or True Positive Rate) Measures the fraction of actual tumor pixels correctly identified:

$$\text{Sensitivity} = \frac{\text{TP}}{\text{TP} + \text{FN}}$$

where

- FN = number of false negative pixels.

- **Specificity** (True Negative Rate) Measures the fraction of non-tumor pixels correctly classified:

$$\text{Specificity} = \frac{\text{TN}}{\text{TN} + \text{FP}}$$

where

- TN = number of true negative pixels.

- **Intersection over Union (IoU)** Also known as the Jaccard index, IoU measures overlap between prediction and ground truth:

$$\text{IoU} = \frac{\text{TP}}{\text{TP} + \text{FP} + \text{FN}}.$$

We report the *mean IoU* (mIoU) averaged over the four classes.

- **Dice Coefficient (F1 Score)** The Dice coefficient emphasizes overlap and is defined as:

$$\text{Dice} = \frac{2 \text{ TP}}{2 \text{ TP} + \text{FP} + \text{FN}}.$$

We compute both the *overall Dice* (averaged across classes) and *per-class Dice* for necrotic/core, edema, and enhancing tissue.

3.4.3 Segmentation Results

In this section, we present the results of our U-Net segmentation model on the BraTS2020 dataset. The model was trained for 50 epochs with a batch size of 16, we will discuss the end results of the training and validation process, including loss and accuracy metrics.

3.4.3.1 Accuracy

The model achieved an impressive pixel-level accuracy of 99.3%, indicating that the vast majority of pixels were correctly classified. This high accuracy is particularly important in medical imaging, where even small errors can have significant implications.

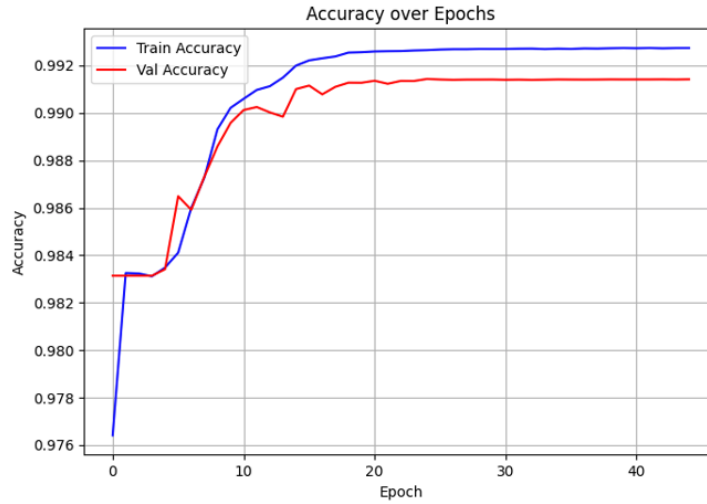


Figure 3.6: Segmentation accuracy over epochs.

3.4.3.2 Loss

The loss function used during training was the categorical cross-entropy loss, which measures the dissimilarity between the predicted and true distributions. The model converged to a low loss of 0.0231, indicating that the predictions were closely aligned with the ground truth.

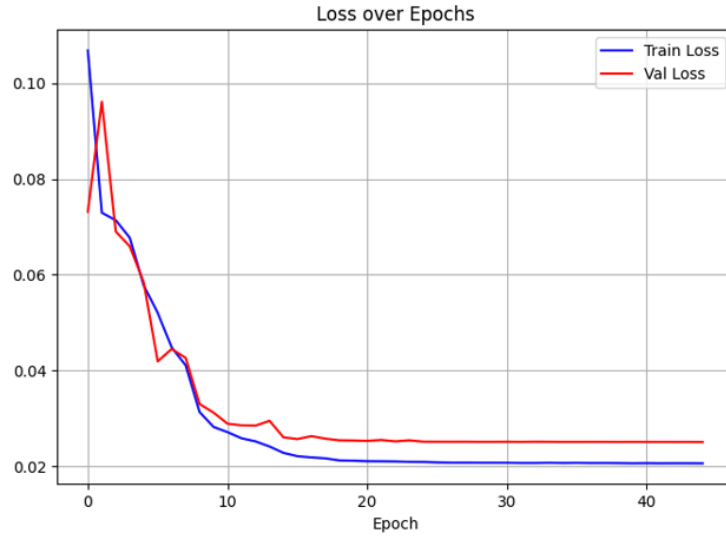


Figure 3.7: Segmentation loss over epochs.

3.4.3.3 Dice Coefficient

The Dice coefficient is a measure of overlap between the predicted and true segmentation masks. The overall Dice coefficient achieved was 58.98%, indicating a good level of agreement between the predicted and true tumor regions. The per-class Dice coefficients were also calculated, providing insights into the model's performance on different tumor subregions.

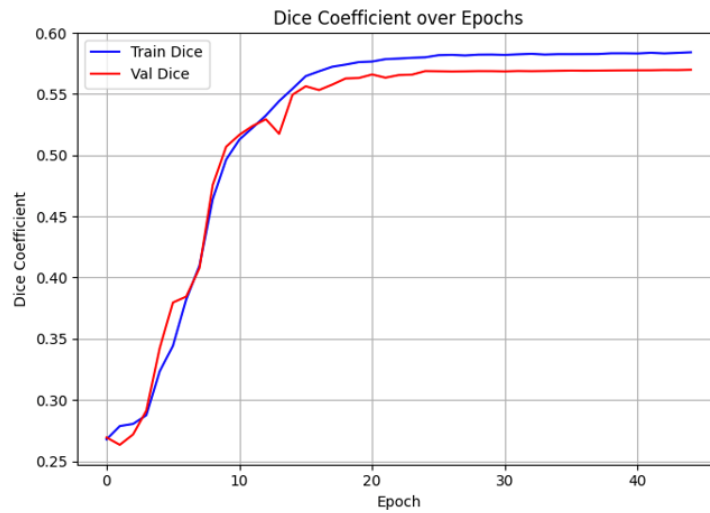


Figure 3.8: Segmentation Dice coefficient over epochs.

3.4.3.4 Mean IoU

The mean Intersection over Union (IoU) was calculated to assess the model's performance across all classes. The mean IoU achieved was 74.66%, indicating a good level of overlap be-

tween the predicted and true segmentation masks. This metric is particularly useful in medical imaging, where accurate delineation of tumor boundaries is crucial for treatment planning.

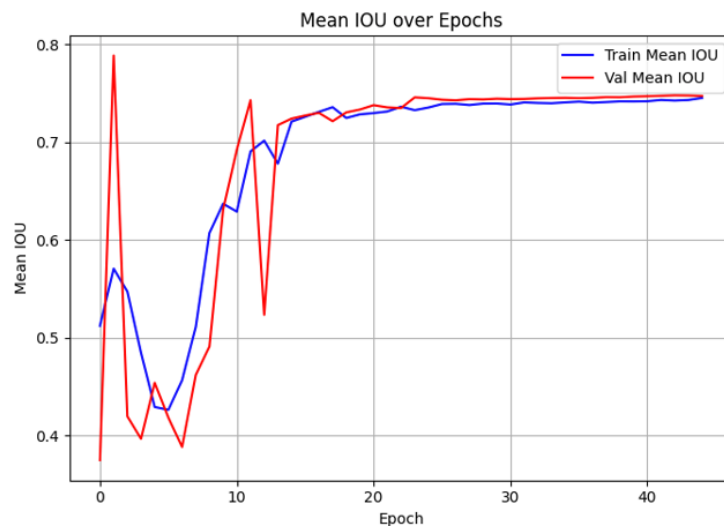


Figure 3.9: Segmentation mean IoU over epochs.

Table 3.1 summarizes the quantitative performance, and Figure 3.10 shows a representative qualitative result.

Table 3.1: Segmentation performance on the test set

Metric	Value
Loss	0.0231
Accuracy	99.30 %
Mean IoU	74.66 %
Dice Coefficient (overall)	58.98 %
Precision	99.37 %
Sensitivity	99.08 %
Specificity	99.79 %

Overall, the model converged to a low loss (0.0231) and achieved excellent pixel-level accuracy (99.3 %), demonstrating strong background discrimination (specificity = 99.8 %). The mean IoU of 74.7 % and overall Dice of 59.0 % indicate reliable overlap between prediction and ground truth also confirms that tumor regions are both accurately and comprehensively detected.

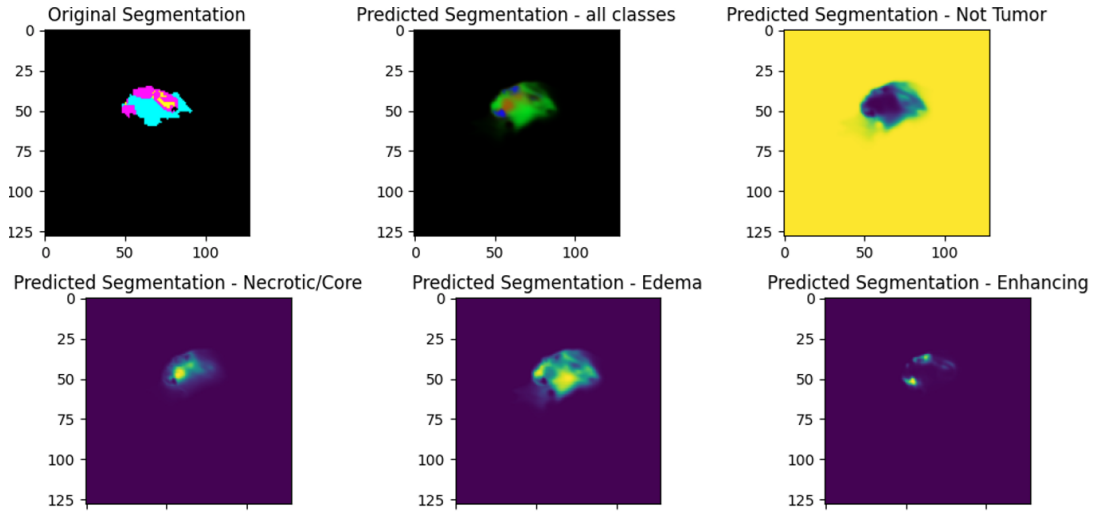


Figure 3.10: Example of segmentation results.

3.5 Classification Module

The classification module distinguishes high-grade gliomas (HGG) from low-grade gliomas (LGG) using handcrafted features extracted from the segmented tumor regions and a support vector machine (SVM) classifier.

3.5.1 Feature Extraction

From each segmented case, we compute the following feature categories:

- **Volume Features:** Volumes of necrotic/core (NCR), edema (ED), enhancing tumor (ET), tumor core (TC), and whole tumor (WT), plus their ratios (e.g., TC/WT, ET/TC).
- **Intensity Statistics:** Mean, standard deviation, minimum, maximum, median, 10th/90th percentiles, and range of voxel intensities for each modality (FLAIR, T1, T1CE, T2) within each tumor component.
- **Texture Features:** Histogram of oriented gradients (HOG)–based descriptors computed on each component.
- **Shape Features:** Extents along each axis, elongation, flatness, and sphericity of the whole tumor mask.
- **Heterogeneity Features:** Contrast between core and edema, and between enhancing and necrotic regions for each modality.

3.5.2 Feature Selection

- Fit a Random Forest classifier on the training split to compute feature importances.
- Select the top 30 most important features for downstream classification.

3.5.3 SVM Model Training

- **Data Split:** 80% training, 20% test (stratified by grade).
- **Scaling:** Standardize features to zero mean and unit variance.
- **Hyperparameter Search:** Grid search over $\{C \in [0.1, 1, 10, 100]\}$, $\gamma \in \{\text{scale, auto, 0.01, 0.1}\}$, and $\{\text{rbf, linear, poly}\}$ kernels, using 5-fold CV.
- **Final Model:** Best-estimator SVM retrained on full training set.

3.5.4 Evaluation Metrics for Classification

We assess performance on the held-out test set using:

- **Accuracy:** Fraction of correctly classified patients.

$$\text{Accuracy} = \frac{\text{TP} + \text{TN}}{\text{TP} + \text{TN} + \text{FP} + \text{FN}}$$

- **Precision, Recall, F1-Score:** Computed per class and averaged.

$$\text{Precision} = \frac{\text{TP}}{\text{TP} + \text{FP}}, \quad \text{Recall} = \frac{\text{TP}}{\text{TP} + \text{FN}}, \quad \text{F1} = \frac{2 \cdot \text{TP}}{2 \cdot \text{TP} + \text{FP} + \text{FN}}$$

- **Confusion Matrix:** Counts of true vs. predicted labels.
- **ROC AUC:** Area under the receiver operating characteristic curve.

$$\text{AUC} = \frac{1}{2} \sum_{i=1}^n (\text{TPR}_i + \text{TPR}_{i-1}) \cdot (\text{FPR}_i - \text{FPR}_{i-1})$$

where n is the number of thresholds and TPR_i and FPR_i are the true positive and false positive rates at the i th threshold.

3.5.5 Classification Results

The SVM classifier was optimized via grid search, yielding the following best hyperparameters:

- $C = 1$, $\gamma = \text{scale}$, Kernel = linear

On the held-out test set (74 patients), the model achieved an overall accuracy of 93.24 %.

Table 3.2: Classification report

Class	Precision	Recall	F1-Score	Support
LGG (0)	86 %	80 %	83 %	15
HGG (1)	95 %	97 %	96 %	59
Accuracy	93.24 %			
Macro avg	90 %	88 %	89 %	74
Weighted avg	93 %	93 %	93 %	74

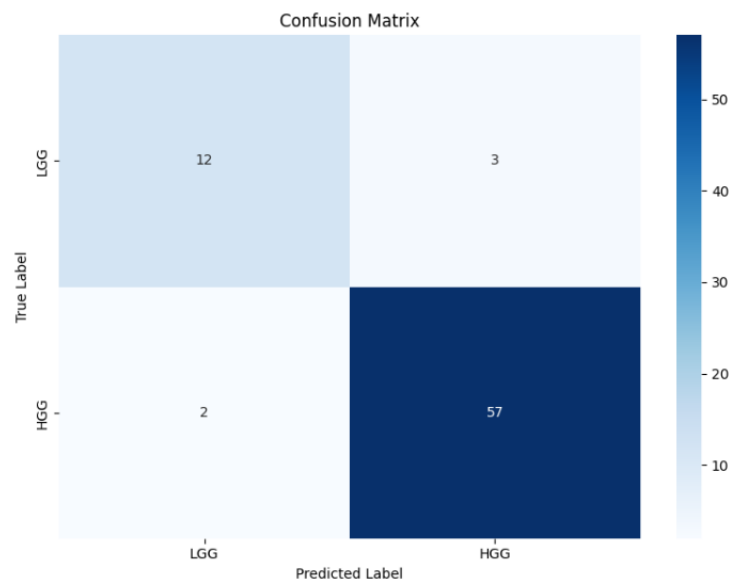


Figure 3.11: Confusion matrix for the SVM classifier.

Example Inference On a new patient (ID 083), the pipeline predicted:

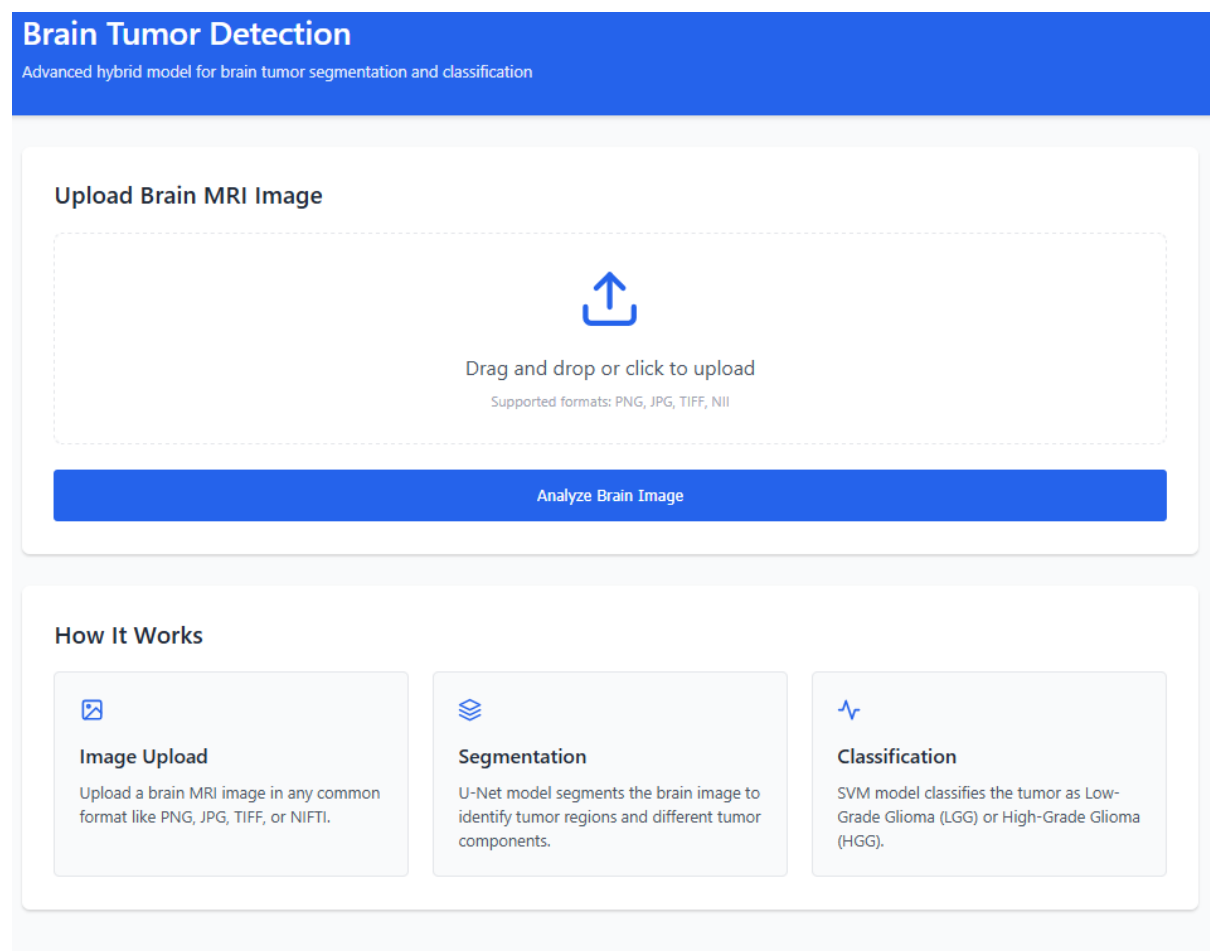
- **Prediction:** HGG
- **Probability of HGG:** 93.60 %
- **Actual Grade:** HGG (correct)

3.6 Application Demo

To illustrate end-user interaction, we developed a lightweight demo application that integrates our trained U-Net and SVM models into a single GUI. The application consists of two main pages:

3.6.1 Upload Page

Presents an HTML form where the user can select and upload a brain tumor image (2D slice). Upon submission, the form sends a POST request to the `/results` route.



The screenshot shows the 'Brain Tumor Detection' application interface. At the top, a blue header bar contains the title 'Brain Tumor Detection' and the subtitle 'Advanced hybrid model for brain tumor segmentation and classification'. Below this, the main content area is divided into two sections. The first section, titled 'Upload Brain MRI Image', features a large dashed box with a blue upload icon (an arrow pointing up into a square) in the center. Below the icon, the text 'Drag and drop or click to upload' is displayed, followed by 'Supported formats: PNG, JPG, TIFF, NII'. A solid blue button labeled 'Analyze Brain Image' is positioned below the upload area. The second section, titled 'How It Works', contains three light gray boxes. The first box, 'Image Upload', shows an image icon and states: 'Upload a brain MRI image in any common format like PNG, JPG, TIFF, or NIFTI.' The second box, 'Segmentation', shows a stack of layers icon and states: 'U-Net model segments the brain image to identify tumor regions and different tumor components.' The third box, 'Classification', shows a pulse line icon and states: 'SVM model classifies the tumor as Low-Grade Glioma (LGG) or High-Grade Glioma (HGG).'

Figure 3.12: Upload page of the application demo.

3.6.2 Results Page

Receives the uploaded image, runs the preprocessing, segmentation (U-Net), feature extraction, and classification (SVM) pipeline, and then renders:

- The original input image.
- The segmentation mask overlaid on the input.
- The predicted tumor grade (LGG/HGG) with its confidence score.

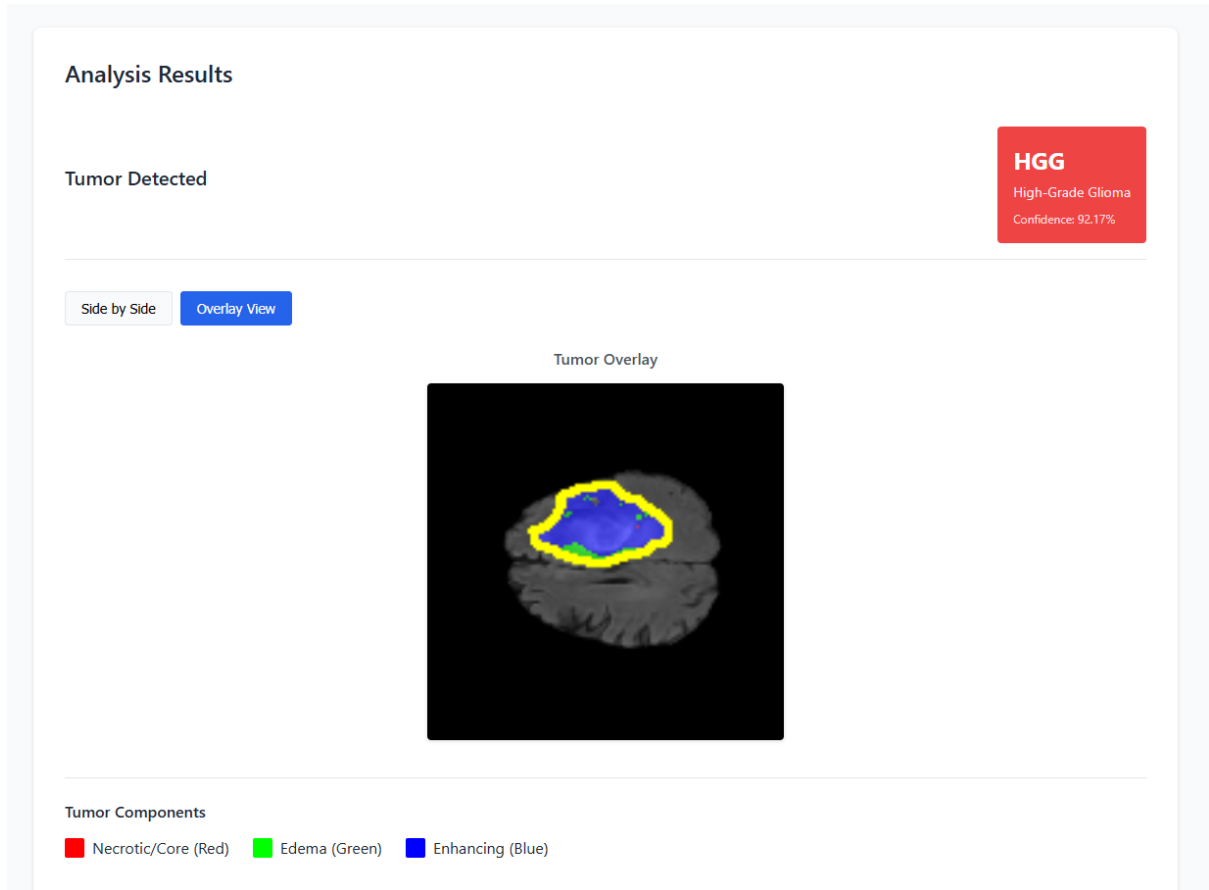


Figure 3.13: Results page of the application demo.

3.7 Conclusion

In this chapter, we have presented a comprehensive methodology for automated brain tumor detection and classification using MR images. Our approach integrates a U-Net-based segmentation model with an SVM classifier, achieving high accuracy and robust performance across multiple evaluation metrics. The segmentation module demonstrated reliable delineation of tumor subregions, while the classification module effectively distinguished between high-grade and low-grade gliomas. Additionally, we showcased the practical application of our framework through a user-friendly demo application, highlighting its potential for real-world clinical use. These contributions underscore the effectiveness of combining deep learning and classical

machine learning techniques in addressing complex medical imaging challenges. Future work could explore further optimization of the pipeline, incorporation of additional data modalities, and validation on larger, more diverse datasets.

General Conclusion

This thesis has explored the development of a hybrid framework for automated brain tumor detection and classification using Magnetic Resonance Imaging (MRI). By integrating deep learning and classical machine learning techniques, we have demonstrated a robust and effective approach to addressing the challenges of brain tumor analysis.

The study began with a comprehensive review of the theoretical foundations, including artificial intelligence, machine learning, and deep learning, with a particular focus on Convolutional Neural Networks (CNNs) and the U-Net architecture. These concepts provided the basis for the segmentation and classification modules of our framework.

The methodology was built upon the BraTS dataset, a benchmark in brain tumor segmentation and classification. We employed a U-Net-based segmentation model to delineate tumor subregions and a Support Vector Machine (SVM) classifier to distinguish between high-grade and low-grade gliomas. The segmentation module achieved an impressive pixel-level accuracy of 99.3%, a mean Intersection over Union (IoU) of 74.66%, and an overall Dice coefficient of 58.98%. These metrics highlight the model's ability to accurately and comprehensively detect tumor regions. The classification module demonstrated strong performance with an overall accuracy of 93.24%.

A key contribution of this work is the integration of these modules into an end-to-end pipeline, capable of processing raw MRI slices to produce segmentation masks and tumor grade predictions. This pipeline was further encapsulated in a user-friendly demo application, showcasing its potential for real-world clinical use.

Despite the promising results, challenges remain. The segmentation module, while accurate, could benefit from further optimization to improve the Dice coefficient and IoU for smaller

tumor subregions. Similarly, the classification module could be enhanced by incorporating additional features or exploring alternative machine learning models. Future work could also focus on expanding the dataset to include more diverse cases, improving generalization across different MRI scanners, and integrating multimodal data for a more comprehensive analysis.

In conclusion, this thesis has demonstrated the feasibility and effectiveness of combining deep learning and classical machine learning techniques for brain tumor analysis. The proposed framework not only advances the state of the art but also lays the groundwork for future research aimed at improving diagnostic accuracy and clinical outcomes in neuro-oncology.

Bibliography

- [1] S. Thakkar. (2020, Feb.) Ai vs ml vs dl: What's the difference? Accessed: 2025-05-09. [Online]. Available: <https://siddhithakkar.com/2020/02/24/ai-vs-ml-vs-dl-whats-the-difference/>
- [2] ScienceDirect Topics, "Artificial intelligence – an overview," <https://www.sciencedirect.com/topics/social-sciences/artificial-intelligence>, accessed: 2025-04-26.
- [3] J. Hurwitz and D. Kirsch, *Machine Learning For Dummies, IBM Limited Edition*. John Wiley & Sons, 2018.
- [4] S. R. Gunn, "Support vector machines for classification and regression," 1998. [Online]. Available: <https://api.semanticscholar.org/CorpusID:120347962>
- [5] O. Ronneberger, P. Fischer, and T. Brox, "U-net: Convolutional networks for biomedical image segmentation," in *International Conference on Medical image computing and computer-assisted intervention*. Springer, 2015, pp. 234–241.
- [6] Verywell Health, "What you should know about mri," <https://www.verywellhealth.com/what-is-an-mri-and-what-does-it-do-3157069>, 2023, accessed: 2023-06-05.
- [7] S. Bauer, R. Wiest, L. P. Nolte, and M. Reyes, "A survey of MRI-based medical image analysis for brain tumor studies," *Physics in Medicine & Biology*, vol. 58, no. 13, p. R97, 2013.
- [8] B. H. Menze, A. Jakab, S. Bauer, J. Kalpathy-Cramer, K. Farahani, J. Kirby *et al.*, "The multimodal brain tumor image segmentation benchmark (BRATS)," *IEEE Transactions on Medical Imaging*, vol. 34, no. 10, pp. 1993–2024, 2015.

- [9] S. Bakas, M. Reyes, A. Jakab, S. Bauer, M. Rempfler, A. Crimi *et al.*, “Identifying the best machine learning algorithms for brain tumor segmentation, progression assessment, and overall survival prediction in the BRATS challenge,” *arXiv preprint arXiv:1811.02629*, 2018.
- [10] L. M. DeAngelis, “Brain tumors,” *New England Journal of Medicine*, vol. 344, no. 2, pp. 114–123, 2001.
- [11] S. Bakas, H. Akbari, A. Sotiras, M. Bilello, M. Rozycki, J. Kirby *et al.*, “Segmentation labels and radiomic features for the pre-operative scans of the TCGA-GBM collection,” The Cancer Imaging Archive, 2019.
- [12] —, “Advancing the cancer genome atlas glioma MRI collections with expert segmentation labels and radiomic features,” *Scientific Data*, vol. 4, p. 170117, 2017.
- [13] F. Isensee, P. F. Jaeger, S. A. Kohl, J. Petersen, and K. H. Maier-Hein, “nnU-Net: A self-configuring method for deep learning-based biomedical image segmentation,” *Nature Methods*, vol. 18, no. 2, pp. 203–211, 2021.
- [14] N. Gordillo, E. Montseny, and P. Sobrevilla, “State of the art survey on MRI brain tumor segmentation,” *Magnetic Resonance Imaging*, vol. 31, no. 8, pp. 1426–1438, 2013.
- [15] S. Bauer, L. P. Nolte, and M. Reyes, “Fully automatic segmentation of brain tumor images using support vector machine classification in combination with hierarchical conditional random field regularization,” in *International Conference on Medical Image Computing and Computer-Assisted Intervention*, 2011, pp. 354–361.
- [16] E. I. Zacharaki, S. Wang, S. Chawla, D. Soo Yoo, R. Wolf, E. R. Melhem, and C. Davatzikos, “Classification of brain tumor type and grade using MRI texture and shape in a machine learning scheme,” *Magnetic Resonance in Medicine*, vol. 62, no. 6, pp. 1609–1618, 2009.
- [17] S. M. S. Reza and K. M. Iftekharuddin, “Multi-class abnormal brain tissue segmentation using texture features,” in *MICCAI Brain Lesion Workshop (BrainLes)*, 2013, pp. 38–42.
- [18] D. Zikic, B. Glocker, E. Konukoglu, A. Criminisi, C. Demiralp, J. Shotton, O. M. Thomas, T. Das, R. Jena, and S. J. Price, “Decision forests for tissue-specific segmentation of

- high-grade gliomas in multi-channel MR,” in *International Conference on Medical Image Computing and Computer-Assisted Intervention*, 2012, pp. 369–376.
- [19] J. Festa, S. Pereira, J. A. Mariz, N. Sousa, and C. A. Silva, “Automatic brain tumor segmentation of multi-sequence MR images using random decision forests,” in *Proceedings of NCI-MICCAI BRATS*, 2013, pp. 23–26.
 - [20] N. J. Tustison, K. L. Shrinidhi, M. Wintermark, C. R. Durst, B. M. Kandel, J. C. Gee, M. C. Grossman, and B. B. Avants, “ANTs and Arboles,” *Proc BRATS Challenge*, pp. 47–50, 2015.
 - [21] V. Simi and J. Joseph, “Segmentation of glioblastoma multiforme from MR images - a comprehensive review,” *Egyptian Journal of Radiology and Nuclear Medicine*, vol. 45, no. 4, pp. 1341–1348, 2014.
 - [22] M. Huang, W. Yang, Y. Wu, J. Jiang, W. Chen, and Q. Feng, “Brain tumor segmentation based on local independent projection-based classification,” *IEEE Transactions on Biomedical Engineering*, vol. 61, no. 10, pp. 2633–2645, 2014.
 - [23] P. Pandit, M. Mandaviya, S. Shah, and N. Shah, “Brain tumor detection using convolutional neural network,” *International Journal of Innovative Technology and Exploring Engineering*, vol. 8, no. 12, pp. 4164–4167, 2019.
 - [24] M. Havaei, A. Davy, D. Warde-Farley, A. Biard, A. Courville, Y. Bengio *et al.*, “Brain tumor segmentation with deep neural networks,” *Medical Image Analysis*, vol. 35, pp. 18–31, 2017.
 - [25] C. Sompong and S. Wongthanavas, “An efficient brain tumor segmentation based on cellular automata and improved tumor-cut algorithm,” *Expert Systems with Applications*, vol. 72, pp. 231–244, 2017.
 - [26] O. Ronneberger, P. Fischer, and T. Brox, “U-Net: Convolutional networks for biomedical image segmentation,” *arXiv preprint arXiv:1505.04597*, 2015.
 - [27] G. Urban, M. Bendszus, F. Hamprecht, and J. Kleesiek, “Multi-modal brain tumor segmentation using deep convolutional neural networks,” in *MICCAI BraTS (Brain Tumor Segmentation) Challenge*, 2014, pp. 31–35.

- [28] S. Pereira, A. Pinto, V. Alves, and C. A. Silva, “Brain tumor segmentation using convolutional neural networks in MRI images,” *IEEE Transactions on Medical Imaging*, vol. 35, no. 5, pp. 1240–1251, 2016.
- [29] Ö. Çiçek, A. Abdulkadir, S. S. Lienkamp, T. Brox, and O. Ronneberger, “3D U-Net: Learning dense volumetric segmentation from sparse annotation,” in *International Conference on Medical Image Computing and Computer-Assisted Intervention*, 2016, pp. 424–432.
- [30] F. Isensee, P. Kickingeder, W. Wick, M. Bendszus, and K. H. Maier-Hein, “No new-net,” in *International MICCAI Brainlesion Workshop*, 2018, pp. 234–244.
- [31] Z. Zhou, M. M. R. Siddiquee, N. Tajbakhsh, and J. Liang, “UNet++: A nested U-Net architecture for medical image segmentation,” in *Deep Learning in Medical Image Analysis and Multimodal Learning for Clinical Decision Support*, 2019, pp. 3–11.
- [32] O. Oktay, J. Schlemper, L. L. Folgoc, M. Lee, M. Heinrich, K. Misawa, K. Mori, S. McDonagh, N. Y. Hammerla, B. Kainz, B. Glocker, and D. Rueckert, “Attention U-Net: Learning where to look for the pancreas,” *arXiv preprint arXiv:1804.03999*, 2018.
- [33] J. Schlemper, O. Oktay, M. Schaap, M. Heinrich, B. Kainz, B. Glocker, and D. Rueckert, “Attention gated networks: Learning to leverage salient regions in medical images,” in *Medical Image Analysis*, vol. 53, 2019, pp. 197–207.
- [34] A. Myronenko, “3D MRI brain tumor segmentation using autoencoder regularization,” in *International MICCAI Brainlesion Workshop*, 2018, pp. 311–320.
- [35] R. McKinley, R. Meier, and R. Wiest, “Ensembles of densely-connected CNNs with label-uncertainty for brain tumor segmentation,” in *International MICCAI Brainlesion Workshop*, 2019, pp. 456–465.
- [36] P. Afshar, A. Mohammadi, and K. N. Plataniotis, “Brain tumor type classification via capsule networks,” in *IEEE International Conference on Image Processing (ICIP)*, 2019, pp. 1570–1574.
- [37] S. Deepak and P. M. Ameer, “Brain tumor classification using deep CNN features via transfer learning,” *Computers in Biology and Medicine*, vol. 111, p. 103345, 2019.

- [38] M. Sajjad, S. Khan, K. Muhammad, W. Wu, A. Ullah, and S. W. Baik, “Multi-grade brain tumor classification using deep CNN with extensive data augmentation,” *Journal of Computational Science*, vol. 30, pp. 174–182, 2019.
- [39] X. Zhao, Y. Wu, G. Song, Z. Li, Y. Zhang, and Y. Fan, “A deep learning model integrating FCNNs and CRFs for brain tumor segmentation,” *Medical Image Analysis*, vol. 43, pp. 98–111, 2018.
- [40] G. Wang, W. Li, S. Ourselin, and T. Vercauteren, “Automatic brain tumor segmentation using cascaded anisotropic convolutional neural networks,” *arXiv preprint arXiv:1709.00382*, 2017.
- [41] K. Kamnitsas, C. Ledig, V. F. Newcombe, J. P. Simpson, A. D. Kane, D. K. Menon *et al.*, “Efficient multi-scale 3D CNN with fully connected CRF for accurate brain lesion segmentation,” *Medical Image Analysis*, vol. 36, pp. 61–78, 2017.
- [42] G. Wang, W. Li, M. Aertsen, J. Deprest, S. Ourselin, and T. Vercauteren, “Aleatoric uncertainty estimation with test-time augmentation for medical image segmentation with convolutional neural networks,” *Neurocomputing*, vol. 338, pp. 34–45, 2019.
- [43] A. Holzinger, C. Biemann, C. S. Pattichis, and D. B. Kell, “What do we need to build explainable AI systems for the medical domain?” *arXiv preprint arXiv:1712.09923*, 2017.
- [44] P. Natekar, A. Kori, and G. Krishnamurthi, “Demystifying brain tumor segmentation networks: Interpretability and uncertainty analysis,” *Frontiers in Computational Neuroscience*, vol. 14, p. 6, 2020.
- [45] A. Lucieri, M. N. Bajwa, S. A. Braun, M. I. Malik, A. Dengel, and S. Ahmed, “On interpretability of deep learning based skin lesion classifiers using concept activation vectors,” in *International Joint Conference on Neural Networks*, 2020, pp. 1–10.
- [46] J. R. Zech, M. A. Badgeley, M. Liu, A. B. Costa, J. J. Titano, and E. K. Oermann, “Variable generalization performance of a deep learning model to detect pneumonia in chest radiographs: A cross-sectional study,” *PLoS Medicine*, vol. 15, no. 11, p. e1002683, 2018.
- [47] R. Shaw, C. H. Sudre, S. Ourselin, and M. J. Cardoso, “Brain tumour segmentation with uncertainty estimation for quality assessment,” *arXiv preprint arXiv:2006.13799*, 2020.

- [48] S. Sedai, D. Mahapatra, S. Hewavitharanage, S. Maetschke, and R. Garnavi, “Semi-supervised learning with semantic knowledge extraction for improved segmentation of brain structures,” *ISPRS Journal of Photogrammetry and Remote Sensing*, vol. 151, pp. 223–232, 2019.
- [49] A. Zhao, G. Balakrishnan, F. Durand, J. V. Gutttag, and A. V. Dalca, “Data augmentation using learned transformations for one-shot medical image segmentation,” *Proceedings of the IEEE/CVF Conference on Computer Vision and Pattern Recognition*, pp. 8543–8553, 2019.
- [50] M. Ghafoorian, A. Mehrtash, T. Kapur, N. Karssemeijer, E. Marchiori, M. Pesteie *et al.*, “Transfer learning for domain adaptation in MRI: Application in brain lesion segmentation,” in *International Conference on Medical Image Computing and Computer-Assisted Intervention*, 2017, pp. 516–524.
- [51] L. Weninger, O. Rippel, S. Koppers, and D. Merhof, “Segmentation of brain tumors and patient survival prediction: Methods for the BraTS 2018 challenge,” *arXiv preprint arXiv:1810.04274*, 2018.
- [52] L. Maier-Hein, M. Eisenmann, A. Reinke, S. Onogur, M. Stankovic, P. Scholz *et al.*, “Why rankings of biomedical image analysis competitions should be interpreted with care,” *Nature Communications*, vol. 9, no. 1, pp. 1–13, 2018.